

AV₃Sb₅ Kagome Superconductors: Progress and Future Directions

Stephen D. Wilson^{1,*} and Brenden R. Ortiz²

¹Materials Department, University of California Santa Barbara, California 93106, USA

²Materials Science and Technology Division, Oak Ridge National Laboratory, Oak Ridge, 37831, Tennessee, USA

*e-mail: stephendwilson@ucsb.edu

ABSTRACT

The recent discovery of the AV₃Sb₅ (A=K, Rb, Cs) kagome superconductors launched a growing field of research investigating electronic instabilities in kagome metals. Specifically, the AV₃Sb₅ family naturally exhibits a Fermi level tuned to the Van Hove singularities associated with the saddle points formed from the prototypical kagome band structure. The charge density wave and superconducting states that form within the kagome networks of these compounds exhibit a number of anomalous properties reminiscent of theoretical predictions of exotic states in kagome metals tuned close to their Van Hove fillings. Here we provide an overview of the key structural and electronic features of AV₃Sb₅ compounds and review the status of investigations into their unconventional electronic phase transitions.

Main text

Introduction

Kagome lattices, networks of corner sharing triangles,¹ have long been crucial building blocks for a range of unconventional states sought in condensed matter physics. Insulating compounds built from kagome networks of localized spins provide extremely rich platforms for studying magnetic frustration and potential spin liquid states predicted to form from the geometric frustration of antiferromagnetic interactions in a kagome network.² Similarly, in metals, the same kagome tiling can lead to interference effects^{3,4} whose details depend on the position of the Fermi level relative to singularities in the electronic band structure.

Specifically, kagome networks generate electronic structures that are known to host bands with particle-hole asymmetric saddle points at electron fillings $f = 5/12$ and $f = 3/12$ on either side of Dirac crossings at $f = 1/3$ as well as a flat band feature.⁵⁻⁷ A form of kinetic frustration due to hopping interference leads to the formation of the localized, flat band that can promote electron-electron interactions. Similarly, for fillings at the saddle points, Van Hove singularities (VHS) result where long-range Coulomb interactions can be promoted due to sublattice interference effects.⁴ These interference effects can generate extraordinarily rich theoretical phase diagrams containing predictions of bond density wave order,^{5,6} orbital magnetism,⁷⁻⁹ pair density wave order,¹⁰ topological insulator phases,^{7,11} and unconventional superconductivity.^{6,12-14}

Recently, considerable interest emerged in finding materials that manifest many of the unconventional electronic states predicted in kagome metals at variable fillings. This involves the identification and study of reasonably two-dimensional metals whose Fermi surfaces/low energy properties are dominated by the electrons occupying their kagome sublattices. One focus is to identify flat band features and systematically find chemistries/perturbations that bring them toward the Fermi level. Notable recent successes observing unusual correlation effects have been reported on this front.¹⁵⁻¹⁷ A second focus is to search for kagome metals possessing electron-fillings near the saddle points within their band structures, similar to those sought in triangular¹⁸ and honeycomb lattices.¹⁹

The VHS accessed at these saddle points generate a logarithmic divergence in the density of states at the M-points (midpoints of the edges) of the Brillouin zone (BZ), and they occur in two different flavors.⁴ The first is the so-called “p-type” VHS whose wave functions derive from a single sublattice within the three-sublattice kagome network, and the second is the so-called “m-type” VHS comprised of wave functions mixed between sublattices. Once the filling corresponding to a VHS is reached, nesting between the three inequivalent M-points across the Fermi surface is predicted to promote a number of charge/spin density wave and superconducting instabilities, with the leading instability dependent on the relative importance of on-site and nearest neighbor Coulomb interactions.⁶

Materials with suitable quasi-two dimensional kagome band structures and fillings near their VHS capable of testing these predictions remained largely elusive until the discovery of the AV₃Sb₅ (A=K, Rb, Cs) class of kagome metals.²⁰ These compounds were first reported in 2019 as a new structure type built from a vanadium-based kagome network that forms a

quasi-two dimensional structure both chemically and electronically. An important feature is that the kagome lattice of vanadium ions in AV_3Sb_5 is “nonmagnetic”, meaning that the electrons on the kagome network are delocalized with no local moments (i.e. they are Pauli paramagnets).^{21,22} This removes energetically favored local moment magnetism that either outcompetes or masks many of the instabilities predicted in a number of kagome lattice Hubbard models. A trivial example is the competition between static magnetic order and superconductivity or the dominant response of local moments when searching for weaker, orbital magnetism.

The goal of this review is to synthesize the experimental progress in understanding the electronic states and phase behaviors identified in the new class of AV_3Sb_5 kagome charge density wave superconductors, where states ranging from orbital antiferromagnetism^{9,23,24} to electronic nematicity²⁵ to pair density wave order²⁶ have been proposed. The key elements of the crystallographic and electronic structures of this materials class are presented first, followed by an overview of the characteristics of the high-temperature charge density wave (CDW) and the low-temperature superconducting (SC) states. The presence of intermediate energy scales or crossovers in select AV_3Sb_5 variants will be reviewed as well as the current state of experiments perturbing both CDW and SC order parameters via chemical substitution and pressure. We view the current review as timely due to the coalescence of much of the experimentally delineated phenomenology surrounding the CDW and SC order parameters in AV_3Sb_5 compounds, and we hope to help focus future measurements probing the microscopic origins of their unconventional electronic properties.

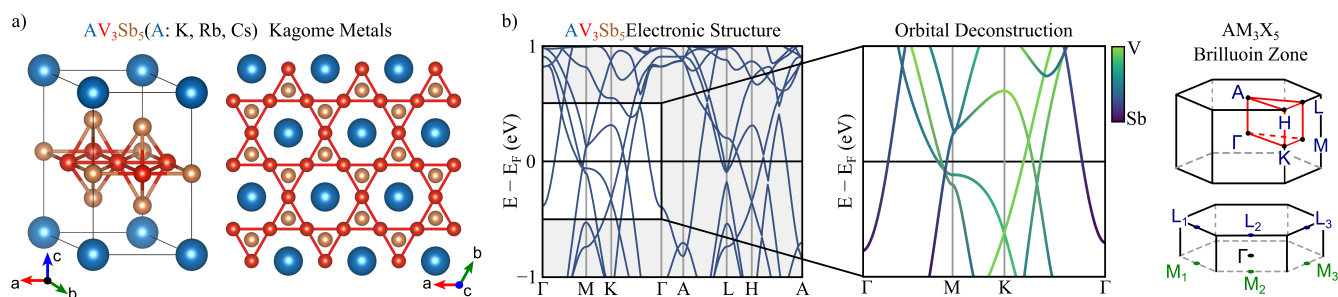


Figure 1. Crystal and electronic band structures of AV_3Sb_5 compounds a | Lattice structure of AV_3Sb_5 with $A=K, Rb, Cs$. Red spheres show the kagome net of V atoms, each coordinated by an octahedra of Sb atoms depicted as gold spheres. Between the V_3Sb_5 layers is a honeycomb lattice of alkali metal A-site atoms, depicted as blue spheres. b | The electronic band structure of AV_3Sb_5 determined via density functional theory calculations. Key features native to the kagome network are highlighted in the $k_z = 0$ plane such as a series of two saddle points with V orbital character just below E_F at the M-point, V-based Dirac points below E_F at the K-point, and a mixed (V,Sb) character saddle point above E_F at the M-point. A representative Brillouin zone (BZ) is also illustrated with the location of high-symmetry points labeled.

Lattice and electronic structures of AV_3Sb_5

Lattice structure

Among the currently popular kagome metal families (e.g. $CoSn$ ^{27–36}, $FeMn_6Ge_6$ ^{37–46}), the AV_3Sb_5 prototype structure is somewhat distinct, as the V-Sb covalent network that forms the hallmark kagome network is intercalated by a honeycomb network of alkali metal ions. Figure 1 shows the normal state crystal structure of the AV_3Sb_5 family. The orthographic perspective shows all bonds with $d < 3 \text{ \AA}$, highlighting the covalent V-Sb sheets and alkali intercalant. The top-down perspective shows only the V-V bonds to highlight the kagome lattice. There are two distinct sublattices of antimony in the AV_3Sb_5 system, and the Sb atom sitting within the kagome network is symmetrically distinct from the Sb atoms above/below the kagome plane.

The well-isolated kagome sheets are one of the most intriguing features of the AV_3Sb_5 family, and the resulting quasi-two dimensional nature most obviously manifests in the mechanical properties. Single crystals are highly exfoliable, and experiments exploring thickness-dependent measurements have been pursued in parallel to studies of bulk crystals,^{47–49} with recent reports claiming to have stable flakes of CsV_3Sb_5 thinned to 5 monolayers.⁵⁰ Such facile exfoliation has made the AV_3Sb_5 family a popular target for surface sensitive probes such as scanning tunneling microscopy (STM) and angle-resolved photoemission (ARPES).

The alkali-atom “intercalation” in the AV_3Sb_5 is not wholly without comparison, as other alkali metal prototypes (e.g. $CsCu_3S_2$,^{51,52} $K_3Cu_3P_2$,⁵³ $Cs_2Pd_3S_4$ ⁵⁴) also exhibit kagome layers separated by alkali atoms. The recently reported families of LnV_3Sb_4 and $LnTi_3Bi_4$ kagome metals also feature slabs of V/Ti kagome networks “intercalated” by rare-earth zig-zag chains.^{55–58} However, many of these layered cousins suffer from more complex unit cells, orthorhombic distortions, or increased

air sensitivity. Remarkably, despite the layered structure and alkali metal intercalant, the AV_3Sb_5 family is highly tolerant of air, water, and common solvents, increasing the overall accessibility of experiments using single crystals.

Together with the quasi-2D mechanical and structural properties, the reduced dimensionality is critical for the realization of the prototypical “kagome” electronic structure. Many other candidate kagome metals are derivatives of the CoSn family (e.g. CoSn, $GdCo_3B_2$, $FeMn_6Ge_6$) or Laves (e.g. $MgZn_2$) prototypes, and maintain a considerable degree of three-dimensional bonding between adjacent kagome layers. Recent computational surveys have highlighted the importance of local bonding and dimensional isolation on the potential to realize the hallmark features of a kagome metal, including the saddle points, Dirac points, and flat bands.⁵⁹

Electronic structure

A schematic showing the representative band structure of AV_3Sb_5 compounds is shown in Figure 1 (b). Across the series of compounds, the band structures are qualitatively similar to one another with bands at the Fermi level dominated by states arising from the kagome nets of vanadium d -states. These are multiorbital materials with d_{xy} , d_{yz} and d_{xz} derived bands forming a series of m-type and p-type VHS at the M-points of the BZ and at energies reasonably close to E_F .^{60–62} Similarly, a Dirac crossing at the K-point of the BZ appears close to E_F in all three compounds.

While electron-phonon coupling likely also plays a role,^{63–66} well-defined nesting at the M-points in the $k_z = \pi$ plane was identified in ARPES measurements.⁶¹ In CsV_3Sb_5 , states identified with the m-type $d_{xz,yz}$ VHS are nearly perfectly nested and gapped below the CDW transition. Optical conductivity data resolve the partial gap that opens below the CDW transition to be $\Delta_{CDW} \approx 60$ meV in KV_3Sb_5 with $T_{CDW} = 78$ K,⁶⁷ $\Delta_{CDW} \approx 78$ meV in CsV_3Sb_5 with $T_{CDW} = 94$ K,⁶⁸ and $\Delta_{CDW} \approx 100$ meV in RbV_3Sb_5 with $T_{CDW} = 104$ K.⁶⁹ This is notably larger than the CDW gaps estimated in surface sensitive STM and ARPES measurements,^{61,70} potentially due to matrix element and surface termination effects.⁷¹

The relative importance of the multiple saddle points close to E_F remains an important area of study; in particular, whether one or multiple VHS are required to capture the essential physics of the CDW state. The ordering of the saddle points below E_F switches due to the modified (expanded) lattice of CsV_3Sb_5 relative to its K- and Rb-based cousins. In DFT models, this relative ordering VHS depends on the interlayer spacing, with KV_3Sb_5 and RbV_3Sb_5 showing a configuration with d_{xz}/d_{yz} -character VHS closest to E_F in the $k_z=0$ plane while CsV_3Sb_5 inverts the order with $d_{x^2-y^2}/d_{z^2}/d_{xy}$ -character VHS closest to E_F .^{68,72} This seemingly coincides with a unique CDW ground state in CsV_3Sb_5 ⁷³ (discussed further in the next section) and suggests that a switch in the orbital character of the Van Hove points closest to E_F impacts the favored charge instability.

While the VHS arising from the kagome sublattice are important for the stabilization of CDW order, additional states at E_F originating from Sb p -orbitals likely also play a role. The large electron pocket at the Γ -point is generated by p -orbitals from the Sb sites in the kagome plane (in the centers of the hexagons of the kagome nets), and an M-point VHS of mixed Sb/V character appears slightly above E_F derived from a mixture of V-states with out-of-plane Sb p -states.⁷⁴ Doping and pressure-based studies described later in this review have shown that removal of the Γ -centered Sb band coincides with the suppression of superconductivity and that small, orbital-selective doping of the Sb bands can dramatically renormalize the CDW state. This phenomenology illustrates that both the VHS from the V d -states in the kagome sublattice as well as Sb p -states are necessary for minimal models of the physics of these compounds, where, for instance, the Sb p -states are proposed to mediate the three-dimensional stacking of the CDW order.^{75,76}

Quantum oscillation measurements confirm the quasi-two dimensional nature of the vanadium bands,^{77–81} and, in the distorted state, a number of low-frequency, CDW-induced vanadium orbits are known to carry a non-trivial Berry phase.^{78,79} These orbits have small effective masses consistent with their originating from partially gapped Dirac bands centered at the K-points, and the role of these nontrivial bands in the superconducting phase remains an open question. Due to the rapid damping of quantum oscillations with increased temperature, measurements of quantum oscillations are largely confined to deep within the CDW state, and more detailed insights are often complicated by the large number of extremal orbits that appear in the reconstructed CDW state.⁸²

A final, salient point regarding the band structure of AV_3Sb_5 is that there exists a continuous, direct band gap and a series of topological bands at the Fermi level. This allows for the assignment of a nontrivial \mathbb{Z}_2 invariant and the classification of these compounds as \mathbb{Z}_2 metals hosting topologically nontrivial surface states.²² These surface states are predicted to be very close to E_F ⁷⁷ at the M-points, and there are experimental hints that they are pulled down to the Fermi level once the band structure is modified through the CDW transition.⁸³ While trivial, bulk states at E_F would mask the impact of these surface states on the low energy properties in the normal state, the protected surface states are potentially important within the superconducting phase where the bulk states become gapped and Fu-Kane (connate) models of topological superconductivity may apply.⁸⁴

Charge density wave order

Real component of bond centered order

AV_3Sb_5 compounds all exhibit CDW order below $T_{CDW} = 78, 104, \text{ and } 94 \text{ K}$ for $A = K, Rb, \text{ and } Cs$ respectively. Though it is difficult to resolve directly, the CDW state is predominantly modeled as deriving from bond-centered order. The main observable is a weak structural distortion of the vanadium sublattice^{22,77,85} that maps into energetically favored breathing modes of the kagome plane.⁶⁰ This distortion is accompanied by a modulation in the local density of states as imaged via STM measurements.^{86–88} A number of initial experimental reports identified that the charge density wave state was three-dimensional with a well-defined phasing between neighboring kagome planes,^{70,77,85} and the in-plane distortion can be characterized by a $3\mathbf{q}$ breathing mode into a "Star-of-David" (SoD) or "Tri-Hexagonal" (TrH) pattern.

Both SoD and TrH patterns are supported by *ab initio* calculations modeling the energetically favored distortions of the kagome plane, with the favored distortions being comprised of M-point modes combined with L-point modes mixing in an out-of-plane modulation to the CDW pattern.^{60,89,90} The result is a staggering of SoD and TrH distortions along the c -axis by shifting one pattern of distortion by half an in-plane lattice constant relative to its neighbors. This staggering along c breaks the in-plane rotational symmetry and results in an orthorhombic unit cell.⁷³ While the relative energies of different distortion types are very close, the commonly predicted distortion mode is the staggered TrH arrangement, comprised of $3\mathbf{q}=(M, L, L)$ modes.

Experimentally, the patterns of charge density wave order differ across the AV_3Sb_5 parent compounds. KV_3Sb_5 and RbV_3Sb_5 share a common staggered TrH distortion,^{73,91,92} while CsV_3Sb_5 seemingly possesses a more complex mixture of TrH and SoD layers staggered relative to one another.^{73,93–95} The average V-V distance ($\approx 2.7 \text{ \AA}$) is the same in the low-temperature charge density wave state of all three compounds, while the room temperature V-V distance expands with the alkali metal cation size. This effect combined with the different ordering of the VHS types near E_F seemingly drives a distinct pattern of CDW order in CsV_3Sb_5 marked by metastability. Specifically, the out-of-plane modulation of TrH/SoD stacking varies as a function of disorder and thermal history, with regions of $2 \times 2 \times 4$ supercells competing with smaller $2 \times 2 \times 2$ supercell regions.⁹⁵ The onset of each of these regions is staged as a function of cooling into the CDW; however, in scenarios where only $2 \times 2 \times 2$ order is isolated, then a staggered TrH CDW state can be determined (similar to the K- and Rb-variants).^{73,94} The experimental observation of mixed TrH and SoD order in the average structure then presumably arises from the $2 \times 2 \times 4$ regions of mixed-state crystals.

Imaginary component of bond centered order

For band fillings close to a p-type VHS, an imaginary CDW state is predicted to stabilize. This is effectively a bond-centered CDW that modulates hopping across the kagome network, creating a form of orbital antiferromagnetism that breaks time-reversal symmetry (TRS). This purely orbital magnetic state exists in the absence of local spins⁹⁶ though it breaks the same symmetries as a spin-density wave. In AV_3Sb_5 compounds, initial hints of TRS-breaking within the CDW state were reported in STM measurements.^{86,88,97} Here, a Fourier transform of the local density of states showed varying weights at the three inequivalent M-point charge superlattice peaks. The application of a magnetic field is reported to switch the relative ordering of the Fourier weights of these peaks (or the effective winding between points), suggesting a chiral CDW state that breaks TRS—an inference stemming via its coupling to an external magnetic field. While the same behavior was reported in all three AV_3Sb_5 variants, there is ongoing debate regarding the repeatability of the effect and its origin. Namely, separate STM studies have failed to resolve a similar magnetic field switching,^{98–100} and there is a debate regarding the surface conditions necessary to resolve the effect versus systematic errors in the measurement protocol. A similar debate exists in optical studies. Here Kerr rotation and circular dichroism initially reported the onset of TRS breaking below the CDW transition of all three AV_3Sb_5 variants;¹⁰¹ however subsequent polar Kerr measurements using a Sagnac interferometer failed to resolve net ferromagnetism or $\mathbf{q}=0$ order.¹⁰²

In contrast to STM and optical measurements, there is remarkable agreement in muon spin relaxation (μSR) studies suggesting TRS breaking within the CDW state.^{103–106} This appears in the form of an order-parameter-like modification in the muon spin relaxation rate suggestive of the appearance of a weak, potentially inhomogeneous local magnetic field. The onset of this local field appears below the CDW transition; however, in CsV_3Sb_5 and RbV_3Sb_5 , there are further modifications observed at lower temperatures. Notably, the magnitude of the local field is small—comparable to nuclear moments in the sample—and traditional oscillations in the muon spin polarization, indicative of long-range magnetic order, are absent. This makes interpretation of the microscopic details driving the depolarization challenging; however, the systematics of the effect, its magnetic field dependence, and the anisotropy of the response strongly suggest that they arise from a subtle TRS-breaking effect.

Magnetotransport measurements are another probe suggesting TRS-breaking in the CDW state. An initial measurement of a large, low-field anomalous Hall effect suggested the onset of magnetic order or spin freezing below the CDW transition in KV_3Sb_5 ¹⁰⁷, and this same effect was subsequently observed in all AV_3Sb_5 variants.^{108,109} This is indicative of the presence of a large Berry flux generated upon entering the CDW state; however, crucially, there is no spontaneous ($\mu_0 H = 0 \text{ T}$) component

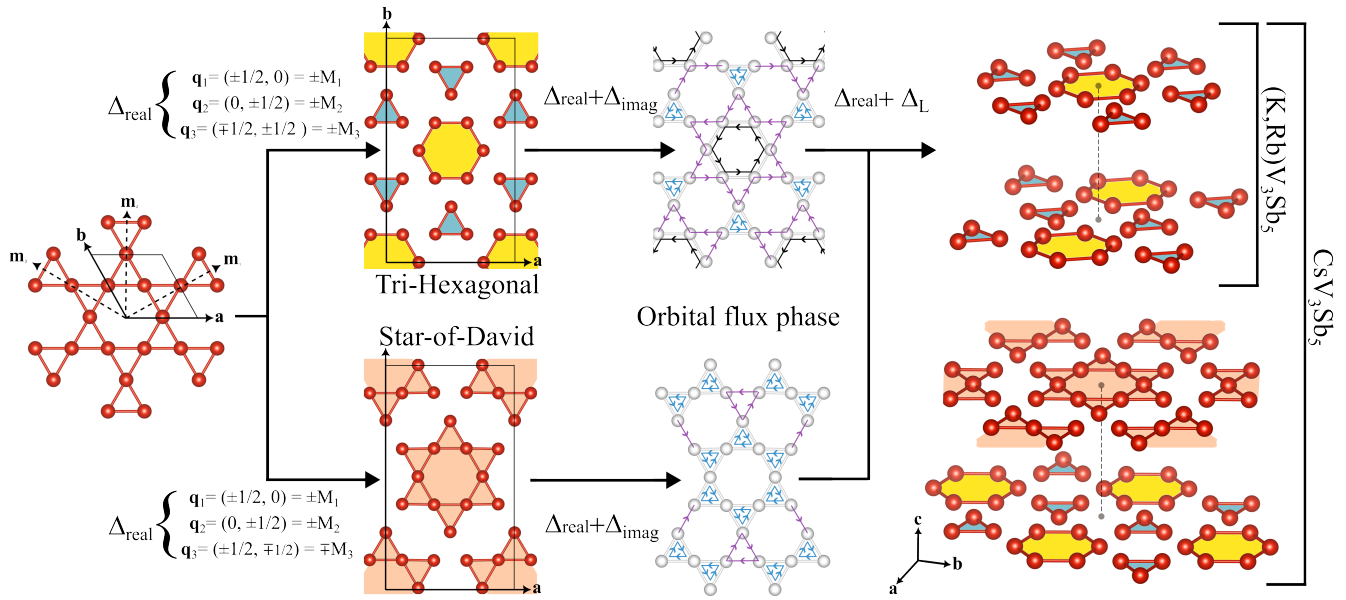


Figure 2. Elements of CDW order in AV_3Sb_5 compounds. The structure of CDW order in AV_3Sb_5 can be thought of a combination of a several key elements. The first element is the primary component of the real order parameter and is the in-plane $3\mathbf{q}$ distortion of the kagome plane, which is favored as breathing into SoD or TrH-type distortions. The second element is the proposed imaginary component, which modulates hopping into an orbital flux phase and breaks TRS. The third element is the interplane correlation that modulates the real component of the CDW state along the c -axis. This arises via consideration of out-of-plane momenta (along the L-points) that modulate the phasing or distortion types between the planes. RbV_3Sb_5 and KV_3Sb_5 each show a TrH in-plane distortion that is staggered by half an in-plane lattice constant along the c -axis. CsV_3Sb_5 has a mixed-phase CDW, whose average 4-layer structure refines to a mixture of staggered TrH distortion interwoven with staggered TrH and SoD distorted layers.

to the anomalous Hall response. The missing zero-field anomalous Hall response is consistent with the absence of a $\mathbf{q}=0$ component of orbital magnetization, and magnetochiral transport studies in CsV_3Sb_5 further suggest field-switchable chirality, rooted either in the structure or broken TRS.¹¹⁰ Recent torque magnetometry data¹¹¹ also report TRS-breaking albeit with an onset temperature higher than T_{CDW} , potentially reflective of the fluctuating/short-range CDW correlations reported at higher temperatures in this compound.^{112,113}

Staged electronic order

A further signature of the unconventional nature of CDW order in AV_3Sb_5 compounds is the appearance of a number of intermediate crossover behaviors below T_{CDW} upon cooling toward the SC phase. Figure 3 illustrates the temperature scales of these anomalies, suggesting a staged evolution of electronic order upon cooling. The vast majority of these reports are reported in CsV_3Sb_5 , with only muon spectroscopy reporting intermediate states in the RbV_3Sb_5 and KV_3Sb_5 compounds.

This difference between compounds likely stems from one of two origins. The first is that the crystal quality of CsV_3Sb_5 is typically superior to that of the other variants, with residual resistivity ratios (RRR) reported as high as 300 (compared to $RRR=60-80$ reported in the Rb- and K-variants).^{81,114,115} This engenders greater exploration by the community, and the lower disorder potentially stabilizes or unmasks subtle experimental signatures of electronic staging in the CDW state. In this scenario, staging of the electronic order is naively present in all three AV_3Sb_5 compounds, but it remains hidden in less frequently studied crystals with poorer quality.

The second possibility is that the subtly different band structure of CsV_3Sb_5 and the change in the relative ordering of VHS close to E_F generates this staging effect. This scenario would imply that the distinct pattern of CDW order and metastability that CsV_3Sb_5 realizes creates a distinct thermal evolution of the CDW state upon cooling. As will be discussed later, CsV_3Sb_5 also possesses distinct doping- and pressure-tuned phase diagrams, suggesting the this second scenario of a unique starting CDW state is the most likely origin for its richer thermal evolution of electronic states.

Focusing on CsV_3Sb_5 , a number of experimental probes report signatures of either lattice or electronic anomalies near $T_a \approx 60$ K and $T_b \approx 35$ K as summarized in the top panel of Figure 3. Each of these temperature scales lacks a sharp thermodynamic anomaly in the heat capacity, suggesting they originate from a subtle crossover in the electronic structure.

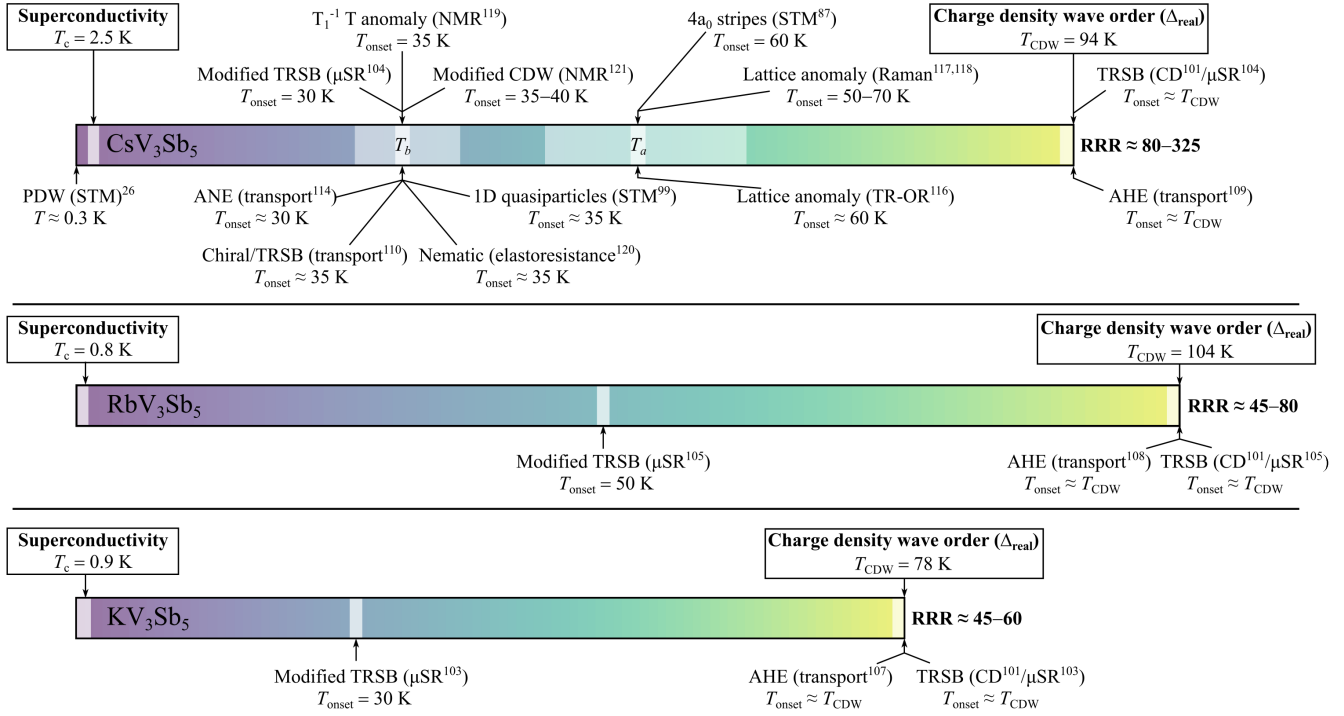


Figure 3. Intermediate electronic phase transitions and crossovers in AV₃Sb₅. The progression of phase transitions and reports of symmetry lowering, such as time reversal symmetry breaking (TRSB), in AV₃Sb₅ compounds. Reports of lattice and electronic anomalies are visually depicted here and described further in the text. The range of reported residual resistivity ratios (RRR $\equiv \rho_{4K}/\rho_{300K}$) for each compound is summarized next to each chart of anomalies. The majority of anomalies intermediate between the onset of CDW order and SC are currently reported in CsV₃Sb₅.

The first anomaly T_a is defined primarily by the emergence of a short-lifetime phonon mode in optics measurements,^{116–118} suggesting that it is coupling to an electronic degree of freedom. T_a also coincides with the appearance of quasi-one dimensional charge stripes with a real space lattice modulation of four lattice constants ($4a_0$) on the surface resolved by STM studies.⁸⁷ Upon further cooling, a second energy scale appears at T_b . This energy scale is characterized by probes reporting rotational symmetry breaking and higher harmonics in magnetotransport, suggestive of the onset of chirality or time reversal symmetry breaking.^{110,114,119,120} Notably, T_b also coincides with the onset of quasi-one dimensional band features in quasi-particle interference spectra⁹⁹ as well as a modification in the local Sb environment¹²¹ and changes in the local magnetic field resolved in muon spin relaxation studies.¹⁰⁴ One potential interpretation is that the T_a energy scale represents the onset of emergent CDW fluctuations that couple to the lattice and slowly freeze toward T_b , affecting a crossover in the electronic structure and transport properties.

One possible driver of staged behavior within the CDW state is the CDW-driven nesting of small pockets in the folded BZ following the onset of CDW order. Figure 4 (a) illustrates one possible scenario where the nested VHS at the M-points in the folded, $P6/mmm$ cell reconstruct the zone via a TrH distortion into a smaller BZ. The reconstructed zone possesses small pockets that nest along a new $\mathbf{q}=\frac{3}{2}\mathbf{M}$ (and equivalent wave vectors) and can drive a secondary instability at lower temperature.¹²² These small pockets were recently observed in a joint STM and ARPES study, and they are proposed to be Chern pockets that support nesting for a new $3\mathbf{q}$ -type order with a real space modulation of $(4a_0/3)$.¹²³

The proposed new $3\mathbf{q}$ wave vector corresponds to the anomalous charge correlations that appear at low-temperature and modulate the superfluid density at the surface as reported in scanning Josephson tunneling measurements.²⁶ This observation has invoked the notion of an intertwined CDW and SC state connected through a primary pair density wave instability.¹⁰ How ubiquitous this phenomenon is in other AV₃Sb₅ compounds, and whether the emergent $4a_0/3$ -type correlations arise from the nearby T_b energy scale remains to be established. Figure 4 (b) summarizes the reports of local charge correlations present in the different material classes and their visualization in STM measurements.

Superconducting order

All three parent AV_3Sb_5 compounds host a superconducting transition within the CDW state, with the highest $T_c = 2.5$ K in CsV_3Sb_5 ²² and $T_c \approx 0.9$ K for $(Rb,K)V_3Sb_5$.^{124,125} Note that the precise T_c reported for each compound varies somewhat between experimental reports (some higher and some lower by a few hundred mK). Due to the competition between SC and the CDW states under slight doping, vetting the “correct” T_c requires detailed parametrization of the CDW state in the same sample. The SC state forms in the clean limit with $l \gg \xi_{ab}$ (where l is the mean free path and ξ is the coherence length),¹²⁶ and the SC state is highly anisotropic with a critical field ratio $H_{c2,c}/H_{c2,ab} \approx 9$.¹²⁷

One of the main challenges in studies of AV_3Sb_5 compounds is to conclusively define the pairing symmetry of the SC order parameter. Despite a number of initial mixed results reporting nodeless versus nodal SC order parameters, the experimental picture has slowly converged to a nodeless,^{126,128} anisotropic¹²⁹ SC gap function with singlet pairing¹³⁰. A multiband, two gap SC state manifests where one gap is substantially smaller than the other^{131,132}—making conventional assessment of low-temperature thermal transport and “U”- versus “V”-shaped SC gap spectra in STM challenging due to quasiparticle contamination from the lower gap. The lower gap size determined via penetration depth measurements is estimated to be $\Delta_{small} \approx 0.5 k_B T_c$ ^{126,129} while the larger gap from tunneling measurements is estimated to range between $\Delta_{large} \approx 2.5 - 3.6 k_B T_c$.^{26,131}

A number of different types of SC are predicted to emerge due to nested VHS in the kagome band structure. A leading instability in many models is for a chiral $d + id$ SC state to emerge.⁴ Such a state would be consistent with the observation of a nodeless SC gap function and reports of broken TRS in the superconducting state;¹⁰⁵ however recent irradiation-based studies of the response of the SC gap to disorder suggest that such a state can be precluded (as well as sign changing s^\pm).¹²⁹ This assessment is based on a conventional picture of a sign-changing gap function being more sensitive to lattice disorder; however recent theoretical models of SC on the kagome lattice suggest that this conventional assumption may not be valid.¹³³ Specifically, the sublattice character of the kagome network near Van Hove fillings renders disorder to be non-pairing breaking for singlet pairing mechanisms irregardless of whether there is a sign change in the gap function. Future work exploring this idea and whether $d + id$ pairing can truly be precluded from existing results is merited.

Upon warming outside of the saturated SC state, additional anomalies are reported at the high temperature phase boundary in the fluctuation regime. Little-Parks measurements probing magnetoresistance oscillations in SC ring devices report an evolution from $2e$ - to $4e$ - to $6e$ -pairing upon warming through the SC transition (where e is the electron charge).¹³⁴ Deep within the SC state, conventional $2e$ oscillations were observed; however these oscillations increase in frequency from $4e$ to $6e$ in a broadened regime of finite resistance. The SC transitions in these devices are substantially broader than those in bulk single crystals, suggesting that disorder/strain imparted during the fabrication process creates an extended fluctuation regime. While these Little-Parks measurements have yet to be replicated, recent mutual inductance measurements report an extended vortex liquid regime in CsV_3Sb_5 ¹³⁵, suggesting that a similar extended fluctuation regime may be accessible in bulk crystals. $6e$ pairing states are predicted to stabilize in such a fluctuation regime in the presence of orbital antiferromagnetism.¹³⁶

Interplay between superconductivity and charge density wave order

The local interplay between charge correlations and the SC state is most extensively visualized in STM measurements, where, at least at the surface and excluding the emergent $\mathbf{q}=\frac{3}{2}$ -type wave vector, there is smooth coexistence of 2×2 -type charge correlations and the SC gap. Perturbing the CDW state via external pressure or chemical doping, however, can have a dramatic

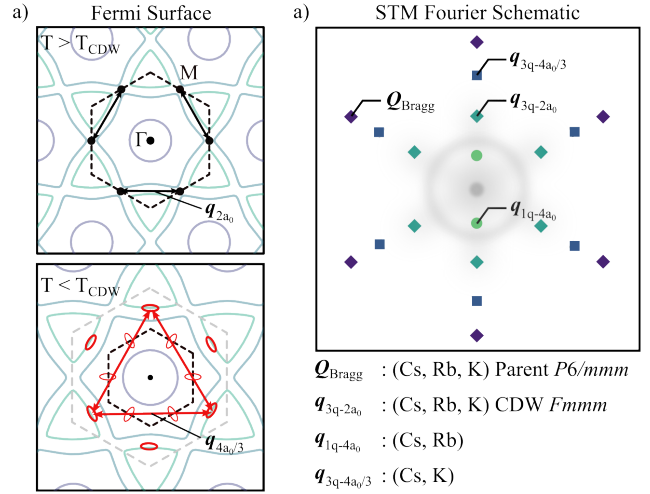


Figure 4. Schematic of momentum space contours of the Fermi surface and corresponding nesting wave vectors for electronic order. a | Nesting wave vectors in the unfolded and folded BZ above and below the CDW transition respectively. Nested M-points are illustrated in the unfolded zone while a schematic of nested Chern pockets are highlighted in the folded zone, below T_{CDW} . b | Wave vectors of charge correlations resolved within the ab -plane as reported via STM measurements and a tabulation of compounds where these correlations have been reported.

effect on the SC phase, which we summarize below.

As alluded to earlier in this paper, the pressure and doping responses of KV_3Sb_5 and RbV_3Sb_5 differ from those of CsV_3Sb_5 . For $(\text{K}, \text{Rb})\text{V}_3\text{Sb}_5$, the application of hydrostatic pressure rapidly suppresses T_{CDW} while simultaneously enhancing T_c .^{138,139} There is a continuous trade-off between the two states, where T_c is enhanced as the CDW state is suppressed and frees up a greater density of states for the SC condensate. The left hand side of Figure 5 (a) shows this common response as the normalized CDW transition temperature for both compounds follows a similar pressure dependence normalized for the critical pressure (P_c) necessary to destabilize CDW order. The suppression of the CDW state eventually terminates in a first-order line where T_c is maximized. The evolution of the SC state up to and across P_c is nearly identical between the two compounds, and a maximal $T_c = 4$ K is realized for both materials once CDW order is suppressed. The conventional trade-off between T_{CDW} and T_c proceeds as pressure naively pushes the Fermi level away from the two occupied VHS closest to E_F as shown in the inset of Figure 5 (a).⁷²

On the right hand side of Figure 5 (a), a distinct pressure-induced response of CsV_3Sb_5 is shown using the same normalized critical pressure and CDW onset temperatures.^{137,142} Pressure again drives a rapid suppression of CDW order that terminates in a first-order line; however T_c evolves in a nonmonotonic manner, forming two SC “domes” within the (P, T) phase diagram. The first dome reaches a peak T_c within the long-range ordered CDW region of the phase diagram. With continued increase in pressure, the CDW is monotonically suppressed, and T_c decreases to close to its zero-pressure value before increasing again to a global maximum near the first-order CDW phase boundary. Moving beyond this boundary with increasing pressure causes T_c to decrease again and form a second, extended “dome”. The termination of the second, higher pressure SC dome seemingly correlates with the removal from the Fermi surface of the Sb p_z states forming the electron-like pocket centered at the Γ -point of the BZ.¹⁴³ The lower pressure dome, in contrast, is likely driven by a CDW transition where charge correlations are weakened as they evolve out of the distinct, parent CDW order in CsV_3Sb_5 into an incommensurate charge density wave state,^{144,145} and partial volume fraction SC is reported near this phase boundary.

Tuning the electron-filling (and thus the Fermi level alignment with the VHS) is another means of studying the interplay between the CDW order and its coupling to the SC state. Figure 5 (b) shows the normalized CDW transitions for all three parent compounds as a function of critical concentrations of hole-doping x_c where x is the number of doped holes per formula unit. As shown in the inset, hole-doping is naively expected to shift the Fermi level closer to occupied VHS in the band structure, though in an orbitally selective manner with the major changes expected in the filling of the Sb-derived Γ -pocket.^{72,140} Again, the relative responses of $(\text{K}, \text{Rb})\text{V}_3\text{Sb}_5$ and CsV_3Sb_5 are distinct.

Looking first at the left side of Figure 5 (b), hole-doping drives a rapid suppression of CDW order in $(\text{K}, \text{Rb})\text{V}_3\text{Sb}_5$, resulting in a common enhancement in T_c up to 4 K.¹⁴¹ On the right hand side of the plot, CsV_3Sb_5 again shows a double-dome-type evolution where T_c first reaches a maximum inside the CDW state followed by a minimum just beyond the first-order phase boundary where CDW order vanishes.¹⁴⁰ Continued hole-doping drives an increase in T_c to a second maximum outside of the

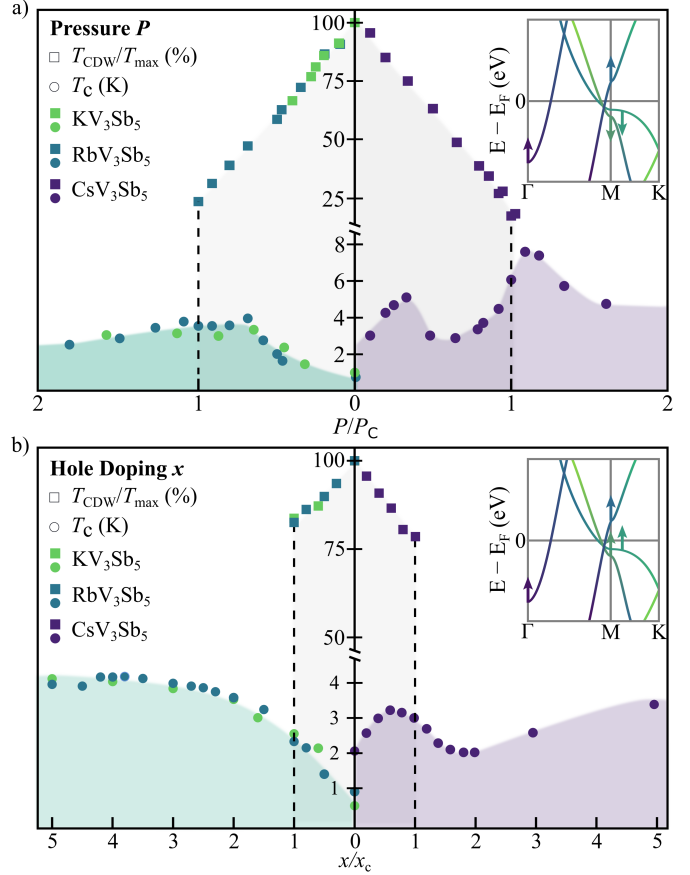


Figure 5. Doping and pressure-tuned phase diagrams of AV_3Sb_5 compounds. a | Pressure-Temperature electronic phase diagram showing the evolution of CDW and SC orders as a function of normalized pressure. The pressure value is normalized by the critical pressure P_c where the CDW state is reported to vanish. b | Electronic phase diagram as a function of normalized hole-doping. Doping concentrations have been normalized by the critical hole-doping value x_c where CDW order nominally vanishes. CDW transition temperatures have been normalized relative to their undoped, ambient pressure values of 100%. Data were adapted from^{137–141}.

CDW state near $x \approx 0.33$. While not shown in Figure 5 (b), continued hole-doping then drives a slight decrease in T_c before SC vanishes in the second dome near $x \approx 0.7$. Again, SC vanishes near the doping concentration where the Sb-derived Γ -pocket is predicted to be lifted above E_F in DFT calculations. These phase diagrams can be most extensively mapped using Sn-atoms as hole-dopants replacing Sb, and qualitatively similar phase diagrams form using Ti-atoms as dopants replacing V,^{146,147} albeit with lower solubility limits and stronger disorder effects.

There are clear commonalities in the (P, T) and (x, T) phase diagrams. For instance, the rapid suppression of the CDW state for all compounds as a function of pressure and hole-doping is uniformly observed and anomalous, in particular given the differing effects on proximities of the VHS to E_F for the two different types of perturbations. The differing response of SC to the suppression of CDW order between CsV_3Sb_5 and $(\text{K,Rb})\text{V}_3\text{Sb}_5$ using both types of perturbations likely arises from the unique starting CDW phase of CsV_3Sb_5 . The charge correlations in the seemingly metastable starting CDW state of CsV_3Sb_5 change in character under small perturbations, driving strong charge fluctuations in the SC state as they evolve. The phase boundary or crossover out of the metastable starting CDW state is one possible origin for the initial low-pressure/low-doping dome in CsV_3Sb_5 .

Incommensurate quasi-one dimensional charge correlations were recently observed near the CDW phase boundary of hole-doped CsV_3Sb_5 suggesting such a crossover may exist.¹⁴⁸ NMR measurements similarly report the presence of incommensurate charge correlations near the boundary between pressure-driven SC domes in this material.¹⁴⁵ Whether or not similar incommensurate charge correlations emerge beyond the CDW phase boundaries of $(\text{K,Rb})\text{V}_3\text{Sb}_5$, however, has yet to be explored. A second commonality in the pressure/doping phase diagrams of CsV_3Sb_5 is the complete suppression of SC once the Sb p_z states are driven away from E_F , suggesting that these states remain essential to stabilizing SC. Furthermore, given that the primary effect on the band structure of both hydrostatic pressure and hole-doping is an orbitally selective modification of the Sb Γ -pocket, the rapid suppression of CDW order in both phase diagrams suggests that the Sb states are intertwined with the V-atom driven CDW order in an unconventional manner. Resonant x-ray scattering measurements have further resolved that Sb states are coupled/hybridized within the CDW transition¹⁴⁹ despite minimal motion of Sb sites through T_{CDW} .

Outlook/Future Perspectives

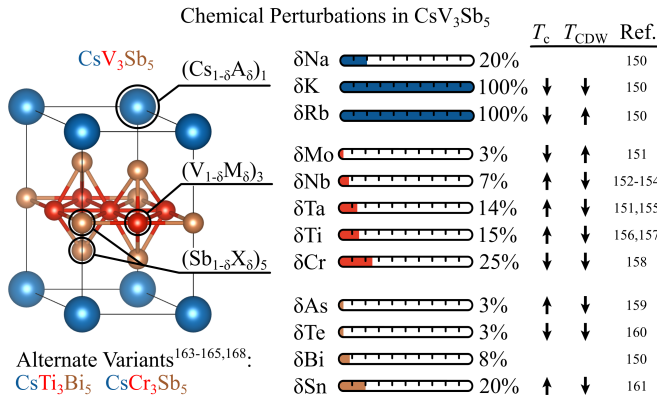


Figure 6. Schematic showing sublattice doping of CsV_3Sb_5 with various electronic, magnetic, and isoelectronic dopants. Percent substitution achievable for dopants on each site of CsV_3Sb_5 and their influence on T_{CDW} and T_c are illustrated.

Considerable effort exploring the chemical flexibility of AV_3Sb_5 compounds both in terms of filling control and in terms of isoelectronic/steric perturbation has been reported.^{147,150-162} A sampling of various chemical substitutions that have been achieved and the corresponding responses of the CDW and SC states for CsV_3Sb_5 is summarized in Figure 6. Where both polycrystalline and single crystal solubility limits are available, deference is given to single crystal results. Generally speaking, solubility limits seem largest in CsV_3Sb_5 , and by far the most research continues to be invested into the Cs-variant of the structure. Site substitution is possible to varying degrees on all sites in the lattice, which provides a valuable litmus for testing the essential band features and interactions necessary for stabilizing the various types of electronic order in these compounds.

Crucially, new parent systems with the same structure type have also been discovered, providing a pristine setting for exploring the impact of forming the same kagome lattice at different fillings. For instance, the recently reported Ti-based variants $(\text{Rb,Cs})\text{Ti}_3\text{Bi}_5$ possess a dramatically different band structure and no signatures of CDW order.¹⁶³⁻¹⁶⁵ There are however reports of an intrinsic rotational symmetry breaking in the quasiparticle spectra of these compounds, suggesting a native nematic electronic instability and continued correlation effects.¹⁶⁶ At lower temperatures, superconductivity was reported in CsTi_3Bi_5 , though there exists a debate whether the SC state is intrinsic or arises from an impurity phase.^{163,167} A new Cr-based variant CsCr_3Sb_5 was also very recently reported with a complex evolution of charge order and potential coexisting, local moment magnetic order.¹⁶⁸ These are exciting developments and suggest further unconventional states can be realized via engineering added interactions across the kagome network of the AM_3X_5 structure-type.

As part of the understanding the origin of the anomalous properties at the band fillings in AV_3Sb_5 , the role of the seemingly nested VHS at E_F in driving the staged phase behavior needs to be further constrained experimentally, and the band features

necessary for a minimal model of their properties need to be determined. In particular, the relative importance of the in-plane and out-of-plane Sb p -states in stabilizing CDW order, SC, or both is an important open question. Other material comparators with similar band fillings may provide clues to this. For instance, kagome net RV_6Sn_6 compounds (R =rare earth), while more three-dimensional, possess similar VHS near their Fermi levels, yet they lack similar phase electronic phase transitions.^{169,170} A crucial difference is likely that the Sn sites are pushed out of the V-based kagome nets, removing a comparable Sn p -pocket at the Γ -point in the BZ.

Going forward, crucial experiments directly resolving the symmetries broken in the CDW state of AV_3Sb_5 are either planned or underway. Whether or not TRS is broken via a bond-centered CDW is a central question and, if confirmed, would represent the first manifestation of orbital antiferromagnetism in the solid state. One likely resolution to experimental discrepancies in resolving a TRS-broken state is the impact of strain on the response of AV_3Sb_5 compounds. While externally applied, in-plane strain has a muted impact on the relative T_c and T_{CDW} values (likely driven via the Poisson ratio),¹⁷¹ strain fields either frozen within crystals or imparted during mounting/cooling samples have recently been shown to have a dramatic impact on the electronic responses associated with TRS- and rotational symmetry breaking.

Specifically, removal/minimization of strain fields within crystals of CsV_3Sb_5 seemingly governs whether rotational symmetry breaking is observable within in-plane charge transport measurements.¹⁷² Furthermore, an applied magnetic field orthogonal to the kagome planes induces in-plane transport anisotropy, suggestive of a piezomagnetic response and a natural coupling of TRS-breaking order to strain. Recent STM measurements directly resolve such a piezomagnetic response as well as optically-induced switching of chirality in the CDW state at the surface of RbV_3Sb_5 crystals.¹⁷³ The emerging picture is then one of a native orbital antiferromagnetic state that breaks TRS and is strongly coupled to out-of-plane magnetic fields and in-plane strain fields.¹⁷⁴ These fields can imbalance the components of the multi-q CDW order and induce a net ferromagnetic or $\mathbf{q}=0$ signal detectable by a number of probes (such as Kerr rotation measurements). Future work exploring the notion of strain's impact on the weak magnetic signal detected in muon spin relaxation and optics measurements is an exciting path forward.

Resolving the above puzzles will provide crucial hints for the pairing symmetry of the lower temperature superconducting state in AV_3Sb_5 compounds and hopefully motivate the search for new materials platforms that host similar band structures. The number of new AM_3X_5 variants recently uncovered is a promising new direction for exploring other correlated states possible on a kagome network. We envision many new opportunities emerging as this new materials phase space is fully explored and the rich frontier of states predicted within kagome metals tuned near their Van Hove fillings can be tested in real materials platforms.

Acknowledgements

S.D.W. gratefully acknowledges support from the UC Santa Barbara NSF Quantum Foundry funded via the Q-AMASE-i program under award DMR-1906325 and the Eddleman Center for Quantum Innovation. B.R.O gratefully acknowledges support from the U.S. Department of Energy (DOE), Office of Science, Basic Energy Sciences (BES), Materials Sciences and Engineering Division.

Author contributions

S.D.W. and B.R.O. composed the manuscript and created the figures.

Competing interests

S.D.W. and B.R.O. declare no competing financial interests in creating this work. Notice: This manuscript has been authored by UT-Battelle, LLC under Contract No. DE-AC05-00OR22725 with the U.S. Department of Energy. The United States Government retains and the publisher, by accepting the article for publication, acknowledges that the United States Government retains a non-exclusive, paid-up, irrevocable, world-wide license to publish or reproduce the published form of this manuscript, or allow others to do so, for United States Government purposes. The Department of Energy will provide public access to these results of federally sponsored research in accordance with the DOE Public Access Plan (<http://energy.gov/downloads/doe-public-access-plan>).

References

1. Syôzi, I. Statistics of kagomé lattice. *Progress of Theoretical Physics* **6**, 306–308 (1951).
2. Norman, M. Colloquium: Herbertsmithite and the search for the quantum spin liquid. *Reviews of Modern Physics* **88**, 041002 (2016).
3. Bergman, D. L., Wu, C. & Balents, L. Band touching from real-space topology in frustrated hopping models. *Phys. Rev. B* **78**, 125104 (2008).
4. Kiesel, M. L. & Thomale, R. Sublattice interference in the kagome hubbard model. *Physical Review B* **86**, 121105 (2012).

5. Wang, W.-S., Li, Z.-Z., Xiang, Y.-Y. & Wang, Q.-H. Competing electronic orders on kagome lattices at van hove filling. *Physical Review B* **87**, 115135 (2013).
6. Kiesel, M. L., Platt, C. & Thomale, R. Unconventional fermi surface instabilities in the kagome hubbard model. *Physical review letters* **110**, 126405 (2013).
7. Wen, J., Rüegg, A., Wang, C.-C. J. & Fiete, G. A. Interaction-driven topological insulators on the kagome and the decorated honeycomb lattices. *Physical Review B* **82**, 075125 (2010).
8. Nayak, C. Density-wave states of nonzero angular momentum. *Phys. Rev. B* **62**, 4880–4889 (2000).
9. Lin, Y.-P. & Nandkishore, R. M. Complex charge density waves at Van Hove singularity on hexagonal lattices: Haldane-model phase diagram and potential realization in the kagome metals AV_3Sb_5 ($A=K, Rb, Cs$). *Physical Review B* **104**, 045122 (2021).
10. Wu, Y.-M., Thomale, R. & Raghu, S. Sublattice interference promotes pair density wave order in kagome metals. *Physical Review B* **108**, L081117 (2023).
11. Guo, H.-M. & Franz, M. Topological insulator on the kagome lattice. *Phys. Rev. B* **80**, 113102 (2009).
12. Yu, S.-L. & Li, J.-X. Chiral superconducting phase and chiral spin-density-wave phase in a hubbard model on the kagome lattice. *Phys. Rev. B* **85**, 144402 (2012).
13. Wu, X. *et al.* Nature of Unconventional Pairing in the Kagome Superconductors AV_3Sb_5 ($A=K,Rb,Cs$). *Phys. Rev. Lett.* **127**, 177001 (2021).
14. Lin, Y.-P. & Nandkishore, R. M. Multidome superconductivity in charge density wave kagome metals. *Phys. Rev. B* **106**, L060507 (2022).
15. Kang, M. *et al.* Topological flat bands in frustrated kagome lattice cosn. *Nature communications* **11**, 4004 (2020).
16. Ye, L. *et al.* A flat band-induced correlated kagome metal. *arXiv:2106.10824* (2021).
17. Huang, H. *et al.* Flat-band-induced anomalous anisotropic charge transport and orbital magnetism in kagome metal cosn. *Phys. Rev. Lett.* **128**, 096601 (2022).
18. Martin, I. & Batista, C. D. Itinerant electron-driven chiral magnetic ordering and spontaneous quantum hall effect in triangular lattice models. *Phys. Rev. Lett.* **101**, 156402 (2008).
19. Nandkishore, R., Levitov, L. S. & Chubukov, A. V. Chiral superconductivity from repulsive interactions in doped graphene. *Nature Physics* **8**, 158–163 (2012).
20. Ortiz, B. R. *et al.* New kagome prototype materials: discovery of KV_3Sb_5 , RbV_3Sb_5 , and CsV_3Sb_5 . *Physical Review Materials* **3**, 094407 (2019).
21. Kenney, E. M., Ortiz, B. R., Wang, C., Wilson, S. D. & Graf, M. J. Absence of local moments in the kagome metal KV_3Sb_5 as determined by muon spin spectroscopy. *Journal of Physics: Condensed Matter* **33**, 235801 (2021).
22. Ortiz, B. R. *et al.* CsV_3Sb_5 : A Z2 Topological Kagome Metal with a Superconducting Ground State. *Phys. Rev. Lett.* **125**, 247002 (2020).
23. Feng, X., Zhang, Y., Jiang, K. & Hu, J. Low-energy effective theory and symmetry classification of flux phases on the kagome lattice. *Phys. Rev. B* **104**, 165136 (2021).
24. Denner, M. M., Thomale, R. & Neupert, T. Analysis of Charge Order in the Kagome Metal AV_3Sb_5 ($A=K,Rb,Cs$). *Phys. Rev. Lett.* **127**, 217601 (2021).
25. Grandi, F., Consiglio, A., Sentef, M. A., Thomale, R. & Kennes, D. M. Theory of nematic charge orders in kagome metals. *Phys. Rev. B* **107**, 155131 (2023).
26. Chen, H. *et al.* Roton pair density wave in a strong-coupling kagome superconductor. *Nature* **599**, 222–228 (2021).
27. Yu, X. *et al.* Near room-temperature formation of a skyrmion crystal in thin-films of the helimagnet FeGe. *Nature materials* **10**, 106–109 (2011).
28. Xie, Y. *et al.* Spin excitations in metallic kagome lattice FeSn and CoSn. *Communications Physics* **4**, 240 (2021).
29. Bak, P. & Jensen, M. H. Theory of helical magnetic structures and phase transitions in MnSi and FeGe. *Journal of Physics C: Solid State Physics* **13**, L881 (1980).
30. Kang, M. *et al.* Dirac fermions and flat bands in the ideal kagome metal FeSn. *Nature materials* **19**, 163–169 (2020).
31. Meier, W. R. *et al.* Flat bands in the CoSn-type compounds. *Physical Review B* **102**, 075148 (2020).

32. Liu, Z. *et al.* Orbital-selective Dirac fermions and extremely flat bands in frustrated kagome-lattice metal CoSn. *Nature communications* **11**, 4002 (2020).
33. Sales, B. C. *et al.* Tuning the flat bands of the kagome metal CoSn with Fe, In, or Ni doping. *Physical Review Materials* **5**, 044202 (2021).
34. Teng, X. *et al.* Magnetism and charge density wave order in kagome FeGe. *Nature Physics* 1–9 (2023).
35. Kang, M. *et al.* Topological flat bands in frustrated kagome lattice CoSn. *Nature communications* **11**, 4004 (2020).
36. Sales, B. C. *et al.* Electronic, magnetic, and thermodynamic properties of the kagome layer compound FeSn. *Physical Review Materials* **3**, 114203 (2019).
37. Arachchige, H. W. S. *et al.* Charge Density Wave in Kagome Lattice Intermetallic ScV₆Sn₆. *Physical Review Letters* **129**, 216402 (2022).
38. El Idrissi, B. C., Venturini, G., Malaman, B. & Fruchart, D. Magnetic structures of TbMn₆Sn₆ and HoMn₆Sn₆ compounds from neutron diffraction study. *Journal of the Less Common Metals* **175**, 143–154 (1991).
39. Ghimire, N. J. *et al.* Competing magnetic phases and fluctuation-driven scalar spin chirality in the kagome metal YMn₆Sn₆. *Science Advances* **6**, eabe2680 (2020).
40. Lee, J. & Mun, E. Anisotropic magnetic property of single crystals RV₆Sn₆ (R= Y, Gd- Tm, Lu). *Physical Review Materials* **6**, 083401 (2022).
41. Peng, S. *et al.* Realizing Kagome Band Structure in Two-Dimensional Kagome Surface States of RV₆Sn₆ (R= Gd, Ho). *Physical review letters* **127**, 266401 (2021).
42. Pokharel, G. *et al.* Electronic properties of the topological kagome metals YV₆Sn₆ and GdV₆Sn₆. *Physical Review B* **104**, 235139 (2021).
43. Pokharel, G. *et al.* Highly anisotropic magnetism in the vanadium-based kagome metal TbV₆Sn₆. *Physical Review Materials* **6**, 104202 (2022).
44. Wang, Q. *et al.* Field-induced topological Hall effect and double-fan spin structure with a c-axis component in the metallic kagome antiferromagnetic compound YMn₆Sn₆. *Physical Review B* **103**, 014416 (2021).
45. Yin, J.-X. *et al.* Quantum-limit Chern topological magnetism in TbMn₆Sn₆. *Nature* **583**, 533–536 (2020).
46. Zhang, X. *et al.* Electronic and magnetic properties of intermetallic kagome magnets RV₆Sn₆ (R= Tb- Tm). *Physical Review Materials* **6**, 105001 (2022).
47. Song, B. *et al.* Competing superconductivity and charge-density wave in kagome metal : evidence from their evolutions with sample thickness. *arXiv:2105.09248* (2021).
48. Wei, X. *et al.* Linear nonsaturating magnetoresistance in kagome superconductor thin flakes. *2D Materials* **10**, 015010 (2022).
49. Wu, Y. *et al.* Nonreciprocal charge transport in topological kagome superconductor CsV₃Sb₅. *npj Quantum Materials* **7**, 105 (2022).
50. Song, Y. *et al.* Competition of superconductivity and charge density wave in selective oxidized CsV₃Sb₅ thin flakes. *Physical review letters* **127**, 237001 (2021).
51. Klepp, K. & Weithaler, C. The crystal structures of CsAu₃S₂, RbAu₃Se₂ and CsAu₃Se₂ and their relationship to the CsCu₃S₂ structure type. *Journal of alloys and compounds* **243**, 1–5 (1996).
52. Burschka, C. CsCu₄S₃ und CsCu₃S₂: Sulfide mit tetraedrisch und linear koordiniertem Kupfer. *Z. anorg. allg. Ohem.* **483**, 65–71 (1980).
53. Savelsberg, G. & SCHAFFER, H. Darstellung und Kristallstruktur von K₃CU₃P₂. *Z. Naturforsch. B* **33**, 590–592 (1978).
54. Bronger, W. & Huster, J. Cs₂Pd₃S₄, ein neuer schichtenstrukturtyp. *Journal of the Less Common Metals* **23**, 67–72 (1971).
55. Ortiz, B. R. *et al.* YbV₃Sb₄ and EuV₃Sb₄ vanadium-based kagome metals with Yb²⁺ and Eu²⁺ zigzag chains. *Phys. Rev. Mater.* **7**, 064201 (2023).
56. Ortiz, B. R. *et al.* Evolution of highly anisotropic magnetism in the titanium-based kagome metals LnTi₃Bi₄ (Ln: La...Gd³⁺, Eu²⁺, Yb²⁺). *arXiv:2308.16138* (2023).
57. Ovchinnikov, A. & Bobev, S. Synthesis, Crystal and Electronic Structure of the Titanium Bismuthides Sr₅Ti₁₂Bi_{19+x}, Ba₅Ti₁₂Bi_{19+x}, and Sr_{5-δ}Eu_δTi₁₂Bi_{19+x} (x=0.5–1.0; δ=2.4, 4.0). *Eur. J. Inorg. Chem.* **2018**, 1266–1274 (2018).

58. Ovchinnikov, A. & Bobev, S. Bismuth as a reactive solvent in the synthesis of multicomponent transition-metal-bearing bismuthides. *Inorg. Chem.* **59**, 3459–3470 (2019).
59. Jovanovic, M. & Schoop, L. M. Simple chemical rules for predicting band structures of kagome materials. *Journal of the American Chemical Society* **144**, 10978–10991 (2022).
60. Tan, H., Liu, Y., Wang, Z. & Yan, B. Charge density waves and electronic properties of superconducting kagome metals. *Phys. Rev. Lett.* **127**, 046401 (2021).
61. Kang, M. *et al.* Twofold van Hove singularity and origin of charge order in topological kagome superconductor CsV₃Sb₅. *Nature Physics* **18**, 301–308 (2022).
62. Hu, Y. *et al.* Rich nature of Van Hove singularities in Kagome superconductor CsV₃Sb₅. *Nature Communications* **13**, 2220 (2022).
63. Luo, H. *et al.* Electronic nature of charge density wave and electron-phonon coupling in kagome superconductor KV₃Sb₅. *Nature Communications* **13**, 273 (2022).
64. Kaboudvand, F., Teicher, S. M., Wilson, S. D., Seshadri, R. & Johannes, M. D. Fermi surface nesting and the Lindhard response function in the kagome superconductor CsV₃Sb₅. *Applied Physics Letters* **120** (2022).
65. Xie, Y. *et al.* Electron-phonon coupling in the charge density wave state of CsV₃Sb₅. *Phys. Rev. B* **105**, L140501 (2022).
66. Ferrari, F., Becca, F. & Valentí, R. Charge density waves in kagome-lattice extended Hubbard models at the Van Hove filling. *Phys. Rev. B* **106**, L081107 (2022).
67. Ece, U., Ortiz, B. R., Wilson, S. D., Dressel, M. & Tsirlin, A. A. Optical detection of the density-wave instability in the kagome metal KV₃Sb₅. *NPJ Quantum Materials* **7** (2022).
68. Uykur, E. *et al.* Low-energy optical properties of the nonmagnetic kagome metal CsV₃Sb₅. *Phys. Rev. B* **104**, 045130 (2021).
69. Wenzel, M. *et al.* Optical study of RbV₃Sb₅: Multiple density-wave gaps and phonon anomalies. *Phys. Rev. B* **105**, 245123 (2022).
70. Liang, Z. *et al.* Three-Dimensional Charge Density Wave and Surface-Dependent Vortex-Core States in a Kagome Superconductor CsV₃Sb₅. *Phys. Rev. X* **11**, 031026 (2021).
71. Huai, L. *et al.* Surface-induced orbital-selective band reconstruction in kagome superconductor CsV₃Sb₅. *Chinese Physics B* **31**, 057403 (2022). URL <https://dx.doi.org/10.1088/1674-1056/ac4f50>.
72. LaBollita, H. & Botana, A. S. Tuning the Van Hove singularities in AV₃Sb₅ (A=K,Rb,Cs) via pressure and doping. *Phys. Rev. B* **104**, 205129 (2021).
73. Kautzsch, L. *et al.* Structural evolution of the kagome superconductors AV₃Sb₅ (A = K, Rb, and Cs) through charge density wave order. *Phys. Rev. Mater.* **7**, 024806 (2023).
74. Jeong, M. Y. *et al.* Crucial role of out-of-plane Sb *p* orbitals in Van Hove singularity formation and electronic correlations in the superconducting kagome metal CsV₃Sb₅. *Phys. Rev. B* **105**, 235145 (2022).
75. Ritz, E. T., Fernandes, R. M. & Birol, T. Impact of Sb degrees of freedom on the charge density wave phase diagram of the kagome metal CsV₃Sb₅. *Phys. Rev. B* **107**, 205131 (2023).
76. Li, H., Liu, X., Kim, Y. B. & Kee, H.-Y. Origin of π -shifted three-dimensional charge density waves in the kagomé metal AV₃Sb₅ (A=Cs, Rb, K). *Phys. Rev. B* **108**, 075102 (2023).
77. Ortiz, B. R. *et al.* Fermi Surface Mapping and the Nature of Charge-Density-Wave Order in the Kagome Superconductor CsV₃Sb₅. *Phys. Rev. X* **11**, 041030 (2021).
78. Fu, Y. *et al.* Quantum Transport Evidence of Topological Band Structures of Kagome Superconductor CsV₃Sb₅. *Phys. Rev. Lett.* **127**, 207002 (2021).
79. Shrestha, K. *et al.* Nontrivial Fermi surface topology of the kagome superconductor CsV₃Sb₅ probed by de Haas–van Alphen oscillations. *Phys. Rev. B* **105**, 024508 (2022).
80. Shrestha, K. *et al.* High quantum oscillation frequencies and nontrivial topology in kagome superconductor KV₃Sb₅ probed by torque magnetometry up to 45 T. *Phys. Rev. B* **107**, 155128 (2023).
81. Shrestha, K. *et al.* Fermi surface mapping of the kagome superconductor RbV₃Sb₅ using de Haas-van Alphen oscillations. *Phys. Rev. B* **107**, 075120 (2023).

82. Broyles, C. *et al.* Effect of the Interlayer Ordering on the Fermi Surface of Kagome Superconductor CsV₃Sb₅ Revealed by Quantum Oscillations. *Phys. Rev. Lett.* **129**, 157001 (2022).
83. Hu, Y. *et al.* Topological surface states and flat bands in the kagome superconductor CsV₃Sb₅. *Science Bulletin* **67**, 495–500 (2022).
84. Fu, L. & Kane, C. L. Superconducting proximity effect and majorana fermions at the surface of a topological insulator. *Phys. Rev. Lett.* **100**, 096407 (2008).
85. Li, H. *et al.* Observation of Unconventional Charge Density Wave without Acoustic Phonon Anomaly in Kagome Superconductors AV₃Sb₅ (A=Rb, Cs). *Phys. Rev. X* **11**, 031050 (2021).
86. Jiang, Y.-X. *et al.* Unconventional chiral charge order in kagome superconductor KV₃Sb₅. *Nature Materials* **20**, 1353–1357 (2021).
87. Zhao, H. *et al.* Cascade of correlated electron states in the kagome superconductor CsV₃Sb₅. *Nature* **599**, 216–221 (2021).
88. Shumiya, N. *et al.* Intrinsic nature of chiral charge order in the kagome superconductor RbV₃Sb₅. *Phys. Rev. B* **104**, 035131 (2021).
89. Christensen, M. H., Birol, T., Andersen, B. M. & Fernandes, R. M. Theory of the charge density wave in AV₃Sb₅ kagome metals. *Phys. Rev. B* **104**, 214513 (2021).
90. Subedi, A. Hexagonal-to-base-centered-orthorhombic 4Q charge density wave order in kagome metals KV₃Sb₅, RbV₃Sb₅ and CsV₃Sb₅. *Phys. Rev. Mater.* **6**, 015001 (2022).
91. Frassinetti, J. *et al.* Microscopic nature of the charge-density wave in the kagome superconductor RbV₃Sb₅. *Phys. Rev. Res.* **5**, L012017 (2023).
92. Kang, M. *et al.* Charge order landscape and competition with superconductivity in kagome metals. *Nature Materials* **22**, 186–193 (2023).
93. Hu, Y. *et al.* Coexistence of trihexagonal and star-of-David pattern in the charge density wave of the kagome superconductor AV₃Sb₅. *Phys. Rev. B* **106**, L241106 (2022).
94. Stahl, Q. *et al.* Temperature-driven reorganization of electronic order in CsV₃Sb₅. *Phys. Rev. B* **105**, 195136 (2022).
95. Xiao, Q. *et al.* Coexistence of multiple stacking charge density waves in kagome superconductor CsV₃Sb₅. *Phys. Rev. Res.* **5**, L012032 (2023).
96. Park, T., Ye, M. & Balents, L. Electronic instabilities of kagome metals: Saddle points and landau theory. *Phys. Rev. B* **104**, 035142 (2021).
97. Wang, Z. *et al.* Electronic nature of chiral charge order in the kagome superconductor CsV₃Sb₅. *Phys. Rev. B* **104**, 075148 (2021).
98. Li, H. *et al.* Rotation symmetry breaking in the normal state of a kagome superconductor KV₃Sb₅. *Nature Physics* **18**, 265–270 (2022).
99. Li, H. *et al.* Unidirectional coherent quasiparticles in the high-temperature rotational symmetry broken phase of AV₃Sb₅ kagome superconductors. *Nature Physics* **19**, 637–643 (2023).
100. Li, H. *et al.* No observation of chiral flux current in the topological kagome metal CsV₃Sb₅. *Phys. Rev. B* **105**, 045102 (2022).
101. Xu, Y. *et al.* Three-state nematicity and magneto-optical kerr effect in the charge density waves in kagome superconductors. *Nature Physics* **18**, 1470–1475 (2022).
102. Saykin, D. R. *et al.* High Resolution Polar Kerr Effect Studies of CsV₃Sb₅: Tests for Time-Reversal Symmetry Breaking below the Charge-Order Transition. *Phys. Rev. Lett.* **131**, 016901 (2023).
103. Mielke, C. *et al.* Time-reversal symmetry-breaking charge order in a kagome superconductor. *Nature* **602**, 245–250 (2022).
104. Khasanov, R. *et al.* Time-reversal symmetry broken by charge order in CsV₃Sb₅. *Phys. Rev. Res.* **4**, 023244 (2022).
105. Guguchia, Z. *et al.* Tunable unconventional kagome superconductivity in charge ordered RbV₃Sb₅ and KV₃Sb₅. *Nature Communications* **14**, 153 (2023).
106. Yu, L. *et al.* Evidence of a hidden flux phase in the topological kagome metal CsV₃Sb₅. *arXiv:2107.10714* (2021).

107. Yang, S.-Y. *et al.* Giant, unconventional anomalous Hall effect in the metallic frustrated magnet candidate, KV₃Sb₅. *Science Advances* **6**, eabb6003 (2020). <https://www.science.org/doi/pdf/10.1126/sciadv.abb6003>.
108. Wang, L. *et al.* Anomalous Hall effect and two-dimensional Fermi surfaces in the charge-density-wave state of kagome metal RbV₃Sb₅. *Journal of Physics: Materials* **6**, 02LT01 (2023). URL <https://dx.doi.org/10.1088/2515-7639/acba46>.
109. Yu, F. H. *et al.* Concurrence of anomalous hall effect and charge density wave in a superconducting topological kagome metal. *Phys. Rev. B* **104**, L041103 (2021).
110. Guo, C. *et al.* Switchable chiral transport in charge-ordered kagome metal CsV₃Sb₅. *Nature* **611**, 461–466 (2022).
111. Asaba, T. *et al.* Evidence for an odd-parity nematic phase above the charge density wave transition in kagome metal CsV₃Sb₅ (2023). [2309.16985](https://doi.org/10.2309.16985).
112. Subires, D. *et al.* Order-disorder charge density wave instability in the kagome metal (Cs,Rb)V₃Sb₅. *Nature Communications* **14**, 1015 (2023).
113. Chen, Q., Chen, D., Schnelle, W., Felser, C. & Gaulin, B. D. Charge Density Wave Order and Fluctuations above T_{CDW} and below Superconducting T_c in the Kagome Metal CsV₃Sb₅. *Phys. Rev. Lett.* **129**, 056401 (2022).
114. Chen, D. *et al.* Anomalous thermoelectric effects and quantum oscillations in the kagome metal CsV₃Sb₅. *Phys. Rev. B* **105**, L201109 (2022).
115. Zhu, C. C. *et al.* Double-dome superconductivity under pressure in the V-based kagome metals AV₃Sb₅ (A=Rb and K). *Phys. Rev. B* **105**, 094507 (2022).
116. Ratcliff, N., Hallett, L., Ortiz, B. R., Wilson, S. D. & Harter, J. W. Coherent phonon spectroscopy and interlayer modulation of charge density wave order in the kagome metal CsV₃Sb₅. *Phys. Rev. Mater.* **5**, L111801 (2021).
117. Wu, S. *et al.* Charge density wave order in the kagome metal AV₃Sb₅ (A=Cs,Rb,K). *Phys. Rev. B* **105**, 155106 (2022).
118. Wulferding, D. *et al.* Emergent nematicity and intrinsic versus extrinsic electronic scattering processes in the kagome metal CsV₃Sb₅. *Phys. Rev. Res.* **4**, 023215 (2022).
119. Song, D. *et al.* Orbital ordering and fluctuations in a kagome superconductor CsV₃Sb₅. *Science China Physics, Mechanics & Astronomy* **65**, 247462 (2022).
120. Nie, L. *et al.* Charge-density-wave-driven electronic nematicity in a kagome superconductor. *Nature* **604**, 59–64 (2022).
121. Luo, J. *et al.* Possible star-of-David pattern charge density wave with additional modulation in the kagome superconductor CsV₃Sb₅. *npj Quantum Materials* **7**, 30 (2022).
122. Zhou, S. & Wang, Z. Chern fermi pocket, topological pair density wave, and charge-4e and charge-6e superconductivity in kagomé superconductors. *Nature Communications* **13**, 7288 (2022).
123. Li, H. *et al.* Small fermi pockets intertwined with charge stripes and pair density wave order in a kagome superconductor. *Phys. Rev. X* **13**, 031030 (2023).
124. Yin, Q. *et al.* Superconductivity and Normal-State Properties of Kagome Metal RbV₃Sb₅ Single Crystals. *Chinese Physics Letters* **38**, 037403 (2021). URL <https://dx.doi.org/10.1088/0256-307X/38/3/037403>.
125. Ortiz, B. R. *et al.* Superconductivity in the Z2 kagome metal KV₃Sb₅. *Phys. Rev. Mater.* **5**, 034801 (2021).
126. Duan, W. *et al.* Nodeless superconductivity in the kagome metal CsV₃Sb₅. *Science China Physics, Mechanics & Astronomy* **64**, 107462 (2021).
127. Ni, S. *et al.* Anisotropic Superconducting Properties of Kagome Metal CsV₃Sb₅. *Chinese Physics Letters* **38**, 057403 (2021). URL <https://dx.doi.org/10.1088/0256-307X/38/5/057403>.
128. Zhong, Y. *et al.* Nodeless electron pairing in CsV₃Sb₅-derived kagome superconductors. *Nature* **617**, 488–492 (2023).
129. Roppongi, M. *et al.* Bulk evidence of anisotropic s-wave pairing with no sign change in the kagome superconductor CsV₃Sb₅. *Nature Communications* **14**, 667 (2023).
130. Mu, C. *et al.* S-Wave Superconductivity in Kagome Metal CsV₃Sb₅ Revealed by 121/123Sb NQR and 51V NMR Measurements. *Chinese Physics Letters* **38**, 077402 (2021). URL <https://dx.doi.org/10.1088/0256-307X/38/7/077402>.
131. Yin, L. *et al.* Strain-sensitive superconductivity in the kagome metals KV₃Sb₅ and CsV₃Sb₅ probed by point-contact spectroscopy. *Phys. Rev. B* **104**, 174507 (2021).

132. Gupta, R. *et al.* Microscopic evidence for anisotropic multigap superconductivity in the CsV₃Sb₅ kagome superconductor. *npj Quantum Materials* **7**, 49 (2022).
133. Holbæk, S. C., Christensen, M. H., Kreisel, A. & Andersen, B. M. Unconventional superconductivity protected from disorder on the kagome lattice. *Phys. Rev. B* **108**, 144508 (2023).
134. Ge, J. *et al.* Discovery of charge-4e and charge-6e superconductivity in kagome superconductor CsV₃Sb₅. *arXiv:2201.10352* (2022).
135. Zhang, X. *et al.* Vortex phase diagram of kagome superconductor CsV₃Sb₅ (2023). [2306.13297](#).
136. Varma, C. M. & Wang, Z. Extended superconducting fluctuation region and 6e and 4e flux-quantization in a Kagome compound with a normal state of 3Q-order (2023). [2307.00448](#).
137. Chen, K. Y. *et al.* Double Superconducting Dome and Triple Enhancement of T_c in the Kagome Superconductor CsV₃Sb₅ under High Pressure. *Phys. Rev. Lett.* **126**, 247001 (2021).
138. Wang, N. N. *et al.* Competition between charge-density-wave and superconductivity in the kagome metal RbV₃Sb₅. *Phys. Rev. Res.* **3**, 043018 (2021).
139. Du, F. *et al.* Pressure-induced double superconducting domes and charge instability in the kagome metal KV₃Sb₅. *Phys. Rev. B* **103**, L220504 (2021).
140. Oey, Y. M. *et al.* Fermi level tuning and double-dome superconductivity in the kagome metal CsV₃Sb_{5-x}Sn_x. *Phys. Rev. Mater.* **6**, L041801 (2022).
141. Oey, Y. M., Kaboudvand, F., Ortiz, B. R., Seshadri, R. & Wilson, S. D. Tuning charge density wave order and superconductivity in the kagome metals KV₃Sb_{5-x}Sn_x and RbV₃Sb_{5-x}Sn_x. *Phys. Rev. Mater.* **6**, 074802 (2022).
142. Yu, F. H. *et al.* Unusual competition of superconductivity and charge-density-wave state in a compressed topological kagome metal. *Nature Communications* **12**, 3645 (2021).
143. Tsirlin, A. A. *et al.* Effect of nonhydrostatic pressure on the superconducting kagome metal CsV₃Sb₅. *Phys. Rev. B* **107**, 174107 (2023).
144. Feng, X. Y. *et al.* Commensurate-to-incommensurate transition of charge-density-wave order and a possible quantum critical point in pressurized kagome metal CsV₃Sb₅. *npj Quantum Materials* **8**, 23 (2023).
145. Zheng, L. *et al.* Emergent charge order in pressurized kagome superconductor CsV₃Sb₅. *Nature* **611**, 682–687 (2022).
146. Sur, Y., Kim, K.-T., Kim, S. & Kim, K. H. Optimized superconductivity in the vicinity of a nematic quantum critical point in the kagome superconductor Cs(V_{1-x}Ti_x)₃Sb₅. *Nature Communications* **14**, 3899 (2023).
147. Yang, H. *et al.* Titanium doped kagome superconductor CsV_{3-x}Ti_xSb₅ and two distinct phases. *Science Bulletin* **67**, 2176–2185 (2022).
148. Kautzsch, L. *et al.* Incommensurate charge-stripe correlations in the kagome superconductor CsV₃Sb_{5-x}Sn_x. *npj Quantum Materials* **8**, 37 (2023).
149. Li, H. *et al.* Discovery of conjoined charge density waves in the kagome superconductor CsV₃Sb₅. *Nature Communications* **13**, 6348 (2022).
150. Ortiz, B. R. *et al.* Complete miscibility amongst the AV₃Sb₅ kagome superconductors: Design of mixed A-site AV₃Sb₅ (A: K, Rb, Cs) alloys. *Physical Review Materials* **7**, 014801 (2023).
151. Liu, M. *et al.* Evolution of superconductivity and charge density wave through Ta and Mo doping in CsV₃Sb₅. *Physical Review B* **106**, L140501 (2022).
152. Li, Y. *et al.* Tuning the competition between superconductivity and charge order in the kagome superconductor Cs(V_{1-x}Nb_x)₃Sb₅. *Physical Review B* **105**, L180507 (2022).
153. Zhou, X. *et al.* Effects of niobium doping on the charge density wave and electronic correlations in the kagome metal Cs(V_{1-x}Nb_x)₃Sb₅. *Physical Review B* **107**, 125124 (2023).
154. Xiao, Q. *et al.* Evolution of charge density waves from three-dimensional to quasi-two-dimensional in Kagome superconductors Cs(V_{1-x}M_x)₃Sb₅ (M = Nb, Ta). *arXiv:2304.01740* (2023).
155. Li, J. *et al.* Strong-coupling superconductivity and weak vortex pinning in Ta-doped CsV₃Sb₅ single crystals. *Physical Review B* **106**, 214529 (2022).
156. Liu, Y. *et al.* Doping evolution of superconductivity, charge order, and band topology in hole-doped topological kagome superconductors Cs(V_{1-x}Ti_x)₃Sb₅. *Physical Review Materials* **7**, 064801 (2023).

157. Hou, J. *et al.* Effect of hydrostatic pressure on the unconventional charge density wave and superconducting properties in two distinct phases of doped kagome superconductors $\text{CsV}_{3-x}\text{Ti}_x\text{Sb}_5$. *Physical Review B* **107**, 144502 (2023).
158. Ding, G., Wo, H., Gu, Y., Gu, Y. & Zhao, J. Effect of chromium doping on superconductivity and charge density wave order in the kagome metal $\text{Cs}(\text{V}_{1-x}\text{Cr}_x)_3\text{Sb}_5$. *Physical Review B* **106**, 235151 (2022).
159. Liu, Y. *et al.* Enhancement of superconductivity and suppression of charge-density wave in As-doped CsV_3Sb_5 . *Physical Review Materials* **6**, 124803 (2022).
160. Capa Salinas, A. N. *et al.* Electron-hole asymmetry in the phase diagram of carrier-tuned CsV_3Sb_5 . *Frontiers in Electronic Materials* **3**, 1257490 (2023).
161. Oey, Y. M. *et al.* Fermi level tuning and double-dome superconductivity in the kagome metal $\text{CsV}_3\text{Sb}_{5-x}\text{Sn}_x$. *Physical Review Materials* **6**, L041801 (2022).
162. Lei, X. *et al.* Band splitting and enhanced charge density wave modulation in Mn-implanted CsV_3Sb_5 . *Nanoscale Advances* **5**, 2785–2793 (2023).
163. Werhahn, D. *et al.* The kagomé metals RbTi_3Bi_5 and CsTi_3Bi_5 . *Zeitschrift für Naturforschung B* **77**, 757–764 (2022).
164. Liu, B. *et al.* Tunable Van Hove Singularity without Structural Instability in Kagome Metal CsTi_3Bi_5 . *Phys. Rev. Lett.* **131**, 026701 (2023).
165. Wang, Y. *et al.* Flat Band and Z2 Topology of Kagome Metal CsTi_3Bi_5 . *Chinese Physics Letters* **40**, 037102 (2023). URL <https://dx.doi.org/10.1088/0256-307X/40/3/037102>.
166. Li, H. *et al.* Electronic nematicity without charge density waves in titanium-based kagome metal. *Nature Physics* 1–8 (2023).
167. Yang, H. *et al.* Titanium-based kagome superconductor CsTi_3Bi_5 and topological states (2022). [2209.03840](https://arxiv.org/abs/2209.03840).
168. Liu, Y. *et al.* Superconductivity emerged from density-wave order in a kagome bad metal. *arXiv:2309.13514* (2023).
169. Pokharel, G. *et al.* Electronic properties of the topological kagome metals YV_6Sn_6 and GdV_6Sn_6 . *Phys. Rev. B* **104**, 235139 (2021).
170. Ishikawa, H., Yajima, T., Kawamura, M., Mitamura, H. & Kindo, K. GdV_6Sn_6 : A Multi-carrier Metal with Non-magnetic 3d-electron Kagome Bands and 4f-electron Magnetism. *Journal of the Physical Society of Japan* **90**, 124704 (2021). <https://doi.org/10.7566/JPSJ.90.124704>.
171. Qian, T. *et al.* Revealing the competition between charge density wave and superconductivity in CsV_3Sb_5 through uniaxial strain. *Phys. Rev. B* **104**, 144506 (2021).
172. Guo, C. *et al.* Correlated order at the tipping point in the kagome metal CsV_3Sb_5 (2023). [2304.00972](https://arxiv.org/abs/2304.00972).
173. Xing, Y. *et al.* Optical Manipulation of the Charge Density Wave state in RbV_3Sb_5 (2023). [2308.04128](https://arxiv.org/abs/2308.04128).
174. Christensen, M. H., Birol, T., Andersen, B. M. & Fernandes, R. M. Loop currents in AV_3Sb_5 kagome metals: Multipolar and toroidal magnetic orders. *Phys. Rev. B* **106**, 144504 (2022).